Int. J. Electrochem. Sci., 11 **(2016)** 126 - 139

International Journal of
ELECTROCHEMICAL
SCIENCE
www.electrochemsci.org

Surface Hardening of Aluminium by Laser alloying with Molybdenum and Zirconium powder

A.P.I. Popoola [1*], *O.S. Fatoba*[1], *H.W. Nkosi*[1], *V.S Aigbodion*[1]

[1]Department of Chemical, Metallurgical and Materials Engineering, Tshwane University of Technology, P.M.B X680, Pretoria, South Africa.0001
[*]E-mail: PopoolaAPI@tut.ac.za

Received: 24 September 2015 / *Accepted:* 10 November 2015 / *Published:* 1 December 2015

Aluminium is one of the common elements that has attracted researcher all over the world because of the light weight to strength, but the hardness values and wear resistance is low which limited usage in the area of applications. This research work is based on the surface hardening of aluminum by laser alloying with binary combinations of molybdenum and zirconium metallic powders. The laser was performed with 4.4 kW Rofin Sinar Nd:YAG. The laser alloyed surfaces produced were characterized using standard techniques. The electrochemical, wear and micro-hardness tests were used to determine the possible area of application. The results showed that laser alloying of aluminium with molybdenum and zirconium metallic powders enhanced the hardness values, wear and corrosion resistance. The hardness values of 6-times and wear resistance of 16-stimes were obtained over the substrate at optimum condition of 50%Mo and 50% Zr, laser power of 4 kW and speed of 1.4 m/min. The various microstructures obtained were the main factor responsible for the improvement in properties. This research work has established that binary combinations of molybdenum and zirconium powders can be used to enhance the properties of laser alloyed aluminium

Keywords: LSA; Hardness, Corrosion rate, Wear; Control.

1. INTRODUCTION

The mechanical, physical and chemical properties of aluminium and its alloy depend greatly on its composition and microstructure [1]. These properties can be improved upon coating using laser surface hardening technique. Aluminum and its alloys, as one of the most used materials, possesses greater advantages when compared to many other metals because of its attractive properties such as light weight, thermal conductivity, electrical conductivity, corrosion resistance and its ease to use [2-6] Laser surface alloying (LSA) is one of the methods that can be used for modification of surface

hardening of aluminium and its alloy. For these reasons, LSA has become resourceful on transformation of chemical and mechanical properties. This involves the melting of the substrate with a high power laser beam while simultaneously depositing an alloying metallic powder on the melt pool formed. A range of unique microstructures are produced as a result of this processing method. These unique microstructures obtained greatly depend on the processing parameter and alloy composition [7]. Many researchers have performed different studies on the hardness improvement of Aluminium. Popoola et al. [8] reported on the laser alloying of aluminium type (AA1200) using titanium diboride and Nickel. Mabhali et al. [9] studied the laser alloying of aluminium with Ti, Ni and SiC powders. They found out that intermetallic phases such as Al_3Ni and Al_4C_3 formed after the laser process enhance the hardness values of the aluminium. Mabhali et al. [10] in other hand used Ni and SiC of different ratio to laser alloyed of aluminium (AA1200). The formation of intermetallic phase such as Al_4C_3 enhances the hardness values to four times.

Moreover, formation of metastable solid solution of Cr, Mo, W, Ti, Zr, Nb and other elements in aluminium has been studied by a number of non-laser deposition techniques and this has formed a theoretical basis for the selection of suitable alloying element additions to promote enhanced resistance to corrosion in aluminium [11]. Under equilibrium processing conditions, elements such as Cr, Mo, W, Ti, Zr, Nb, with a known passivating effect on the progress of corrosion in aluminium is either insoluble or nearly insoluble in the metal and hence techniques for their incorporation in non-equilibrium concentrations are required [12]. Since during laser alloying the cooling rate during resolidification of melted surface layers is high, compared with conventional alloying techniques [13, 14] the technique can be employed to produce such non-equilibrium microstructures through increased cooling rates from molten state. Based on the abovementioned, this research is aimed at studying the effect of laser processing parameter on the properties of aluminium AA1200 (control) using Zirconium and molybdenum powders

2. MATERIALS AND METHOD

2.1. Materials

The aluminium of type AA1200 (control) with the chemical composition showed in Table 1 was used as substrate. An aluminium dimension plate of 100 x 100 x 6 mm was achieved through cutting the bulk aluminium material. The machined plates were sand blasted prior to LSA to increase the laser beam absorption and to achieve a clean surface. Molybdenum and Zirconium metallic powders were mixed in 50% to 50% ratio respectively.

Table 2. Chemical composition of the substrate (control)

Element	Al	Fe	Cu	Si
Composition (wt%)	Balance	0.59	0.13	0.12

2.2. Laser Surface Alloying (LSA)

The laser process was conducted using the processing condition in Table 2. A Rofin Sinar continuous wave Nd:YAG laser machine was used. The mix ratio of 50%Mo:50%Zr were fed through the nozzle of the Nd:YAG laser. The mixture was injected into the melt pool created by the laser beam on the substrate. The overlapping of melt tracks obtained was 70%.

Table 2: Laser processing parameter used.

Sample no	Alloying element	Power (kW)	Beam diameter (mm)	Laser Scan speed (m/min)	Powder feed rate (g/min)	Shielding gas	Shield gas flow (L/min)
AMZ3	Mo + Zr	4	3	1.4	3	Argon	4
AMZ4	Mo + Zr	4	3	1.6	3	Argon	4
AMZ5	Mo + Zr	4	3	1.8	3	Argon	4

2.3. Microhardness test

Vickers micro-hardness tester (model FM700) was used in the determination of the hardness values of the samples. The hardness was conducted on the cross section of the samples using a load of 100g, time 10second and 100-150μm spacing between the indentations. Five indentations were taking and the average values were recorded.

2.4. Wear resistance test

The wear tests of the samples were performed using three body abrasive wear tester. A sample dimension of 65x25mm, load of 25N, time 30minutes and Roflfe's silica sand of particle size 0f 300-600μm at a flow rate of 4.3g/s were used for the wear test.

2.6. Microstructure and phase analyses

Before the analysis the surface were grinded with grit papers of 345 to 1000μm and polished with alumina paste. The samples were etched with keller's reagent. Optical and scanning electron microscope equipped with energy dispersive spectrometer were used for the microstructural analysis. The X'Pert Pro model diffractometer was used to identify the various phases presence. A Cu Kα radiation, 45kA and 40mA was used for the scan from 10^o and 100^o (2θ) degrees.

2.7. Electrochemical test

Electrochemical test was performed in a $1cm^2$ area sample surface. All samples were cold mounted to a $1cm^2$ area using the epoxy resins. The samples were then grinded to 600 grit with SiC

grinding papers. Corrosion resistance tests of the samples were done through the linear potentiodynamic polarization test. Measurements were done using the Autolab potentiostat with a computer installed version 1.8 Nova software package. 3.65 wt.%NaCl solution was used for corrosion test. The electrochemical cell consist of three electrodes namely the working electrode (samples), counter electrode (graphite rod) and the platinum rod as a reference electrode. The corrosion potential (E_{corr}), polarization resistance (R_p) and corrosion rate were determined using a scan rate of 0.0015V s^{-1} from a potential of 1.0 V to -2.5 V.

3. RESULTS AND DISCUSSION

3.1. Characterization of the starting materials

Figure 1 shows the SEM micrograph of the substrate where the surface morphology can be clearly seen. The SEM microstructure of the zirconium (Zr) is shown in Figure 2a and it can be seen that the shape of the particles were irregular and flakey granule with inconsistent particle sizes. The XRD pattern of Zr powder clearly indicates that only Zr phase was present (see Figure 2b).

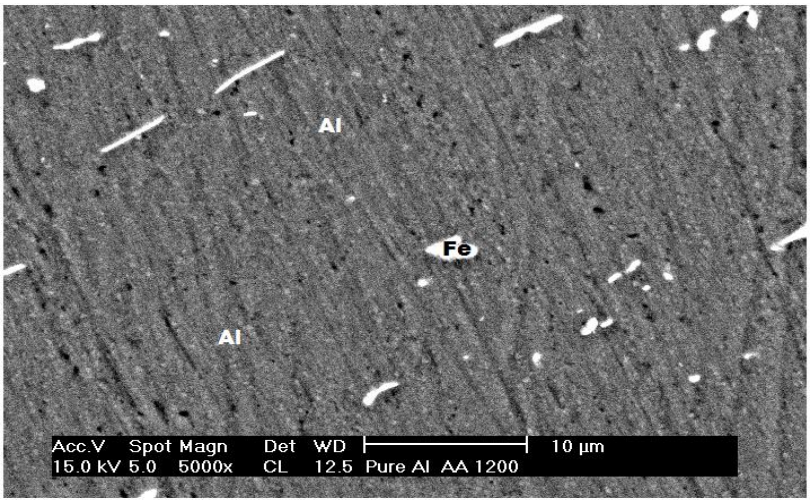

Figure 1. SEM microstructure of the substrate (Control)

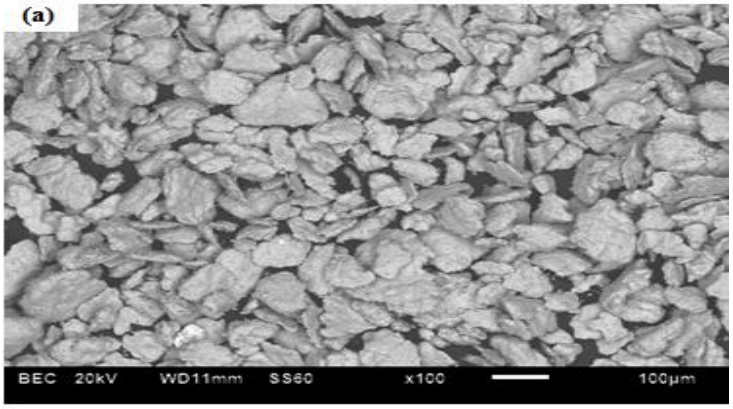

Figure 2a. SEM microstructure of Zirconium (Zr) powder

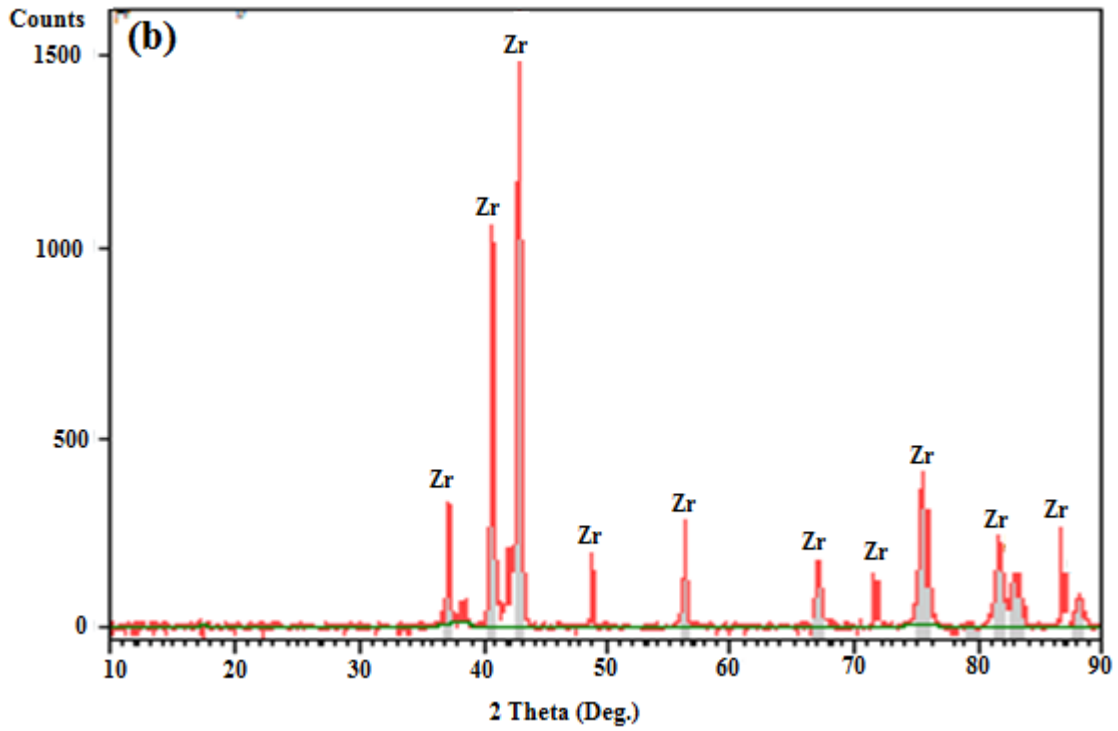

Figure 2b. XRD patterns of Zirconium (Zr) powder.

Figure 3 represents the SEM micrograph of Molybdenum powder used for alloying. Mo powder is spherical in shape.

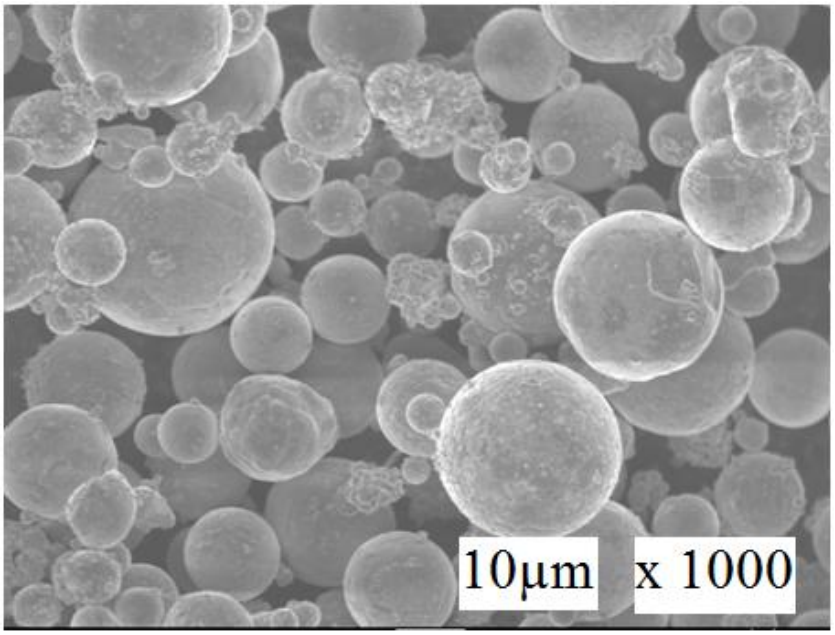

Figure 3. SEM micrograph of Mo powder.

3.2. Microstructure of the LSA AA1200

Laser surface alloying resulted in the formation of different intermetallic phases which led to the effective change of the surface properties of the laser coating formed. The XRD spectrum of the alloyed layers is shown in Figure 4 with the presence of intermetallics Al_2Zr_4 and MoO_3.

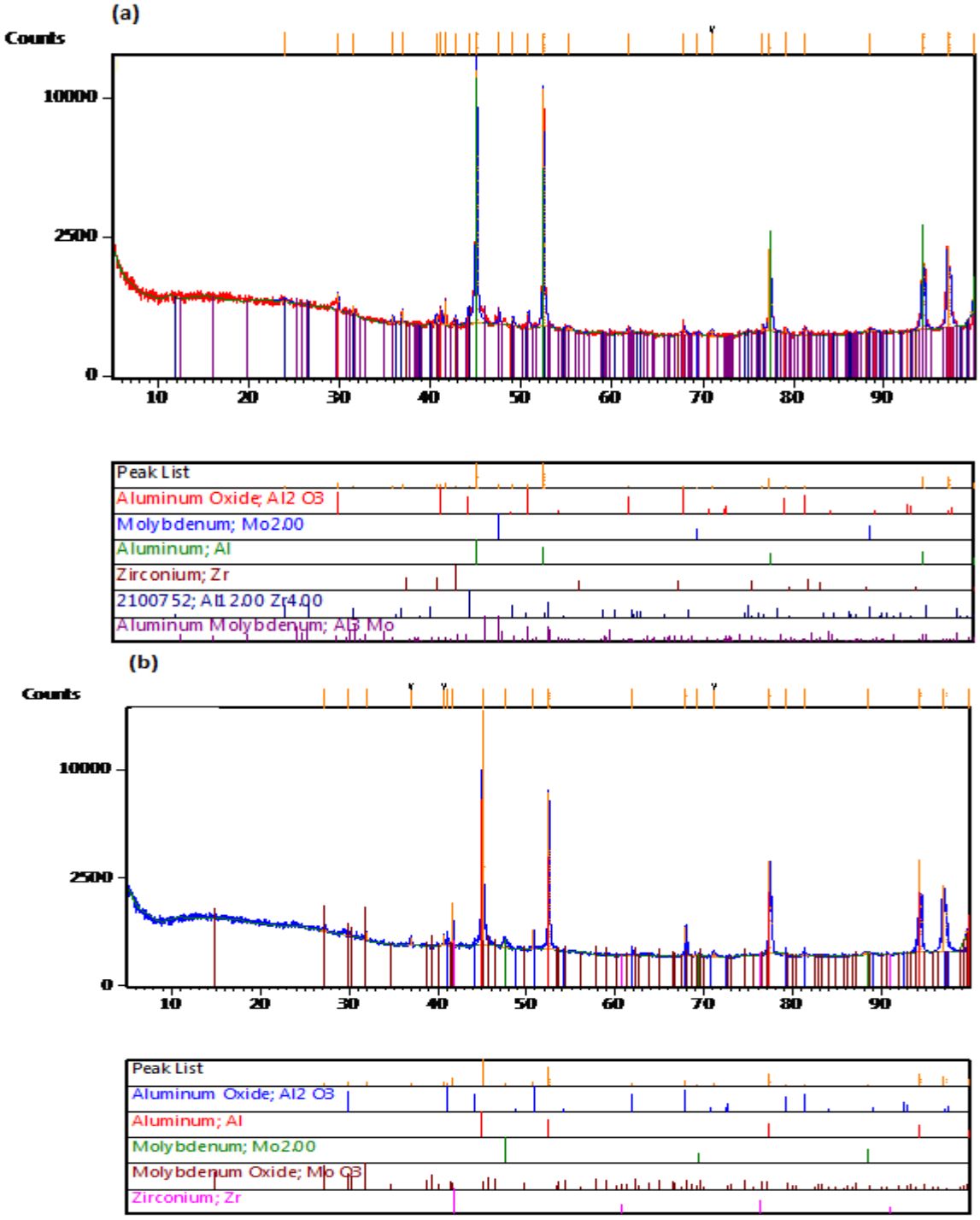

Figure 4. XRD spectrum (a) AMZ 3(b) AMZ 4

The typical optical micrographs of the microstructures of sample AMZ 3 and AMZ 4 are shown in Figure 5. The micrographs of the alloyed surface were observed to have similar microstructures.

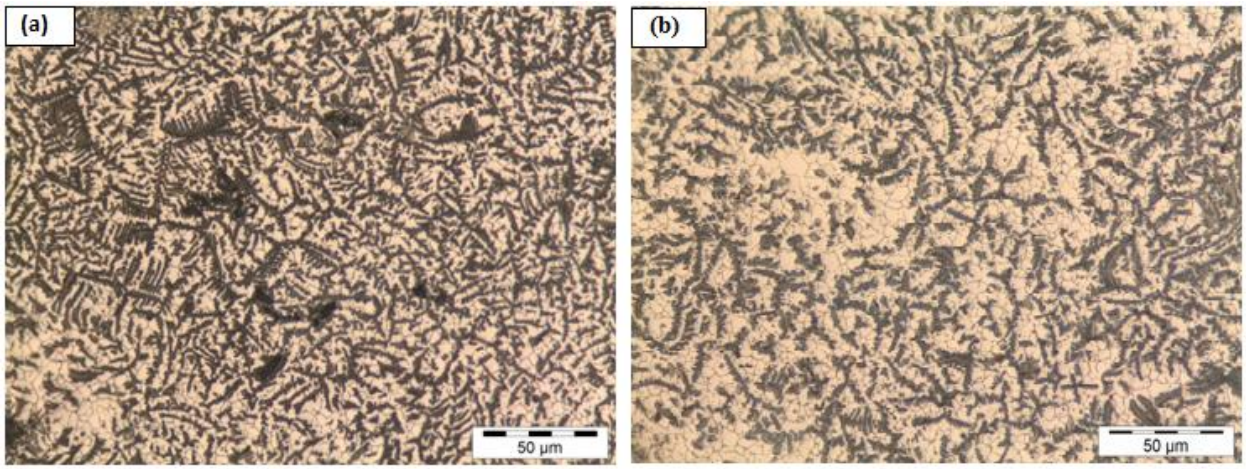

Figure 5. Typical optical micrograph of alloyed surface (a) AMZ 3 and (b) AMZ 4

Figure 6 showed the SEM micrograph of the AMZ 3 sample. It can be observed that laser surface alloying of the control at constant laser power and different laser scanning speeds resulted in the formation of fine dendrite microstructures on the surface as it can be seen from Figure 6. It is evidence from microstructure in Figure 7, that alloying with a mixture of Mo and Zr metallic powders results in the formation of dendrites microstructures. A well dissolution of the metallic powders into the molten aluminium substrate was accomplished due to the high temperatures achieved. The difference in the microstructures of the alloyed layers is as a result of the reactions occurring between the added alloying powder mixture and the substrate and the laser processing parameters.

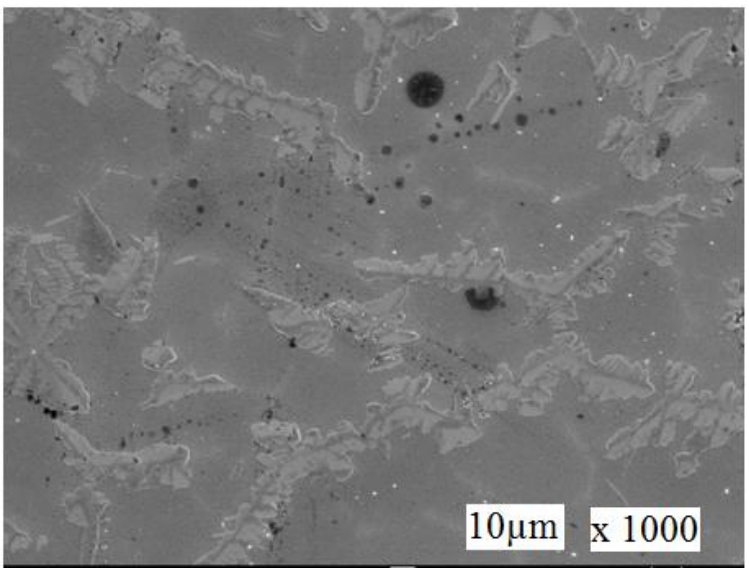

Figure 6. SEM micrograph of AMZ 3.

The laser surface alloyed layer showing dendrite microstructure can be seen from SEM micrograph of sample AMZ 4 in Figure 7. The composition of the alloyed layer at different areas was determined by EDS to be: 99wt% Mo and 1wt% Al, 100wt% Al and (72wt% Al, 16wt% Zr and 12wt%Mo) in area 1, 2 and 3 respectively.

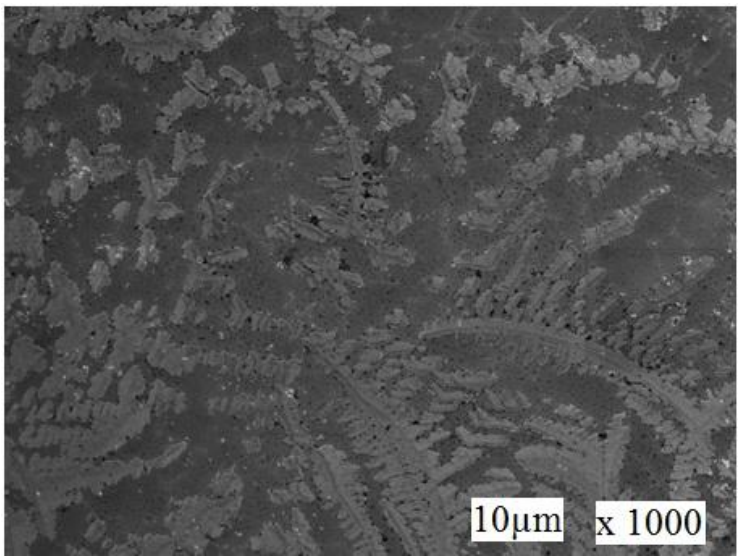

Figure 7. SEM microstructure of AMZ 4.

The concentration profile of the various elements contained within the alloyed layer determined by EDS is showed in Figure 8. In area 1, 99wt% Mo was analyzed and this indicates un-melted Mo particles. The unmelted Mo particles were as the result of the laser processing temperature. Mabhali et al. [10] performed a study on the temperature during laser processing and found out that the temperature was 2362^{o}C while molybdenum melts at 2632^{o}C. Area 2 contained 100wt% Al and in area 3, 72wt% Al, 16wt% Zr and 12wt%Mo elements were analyzed.

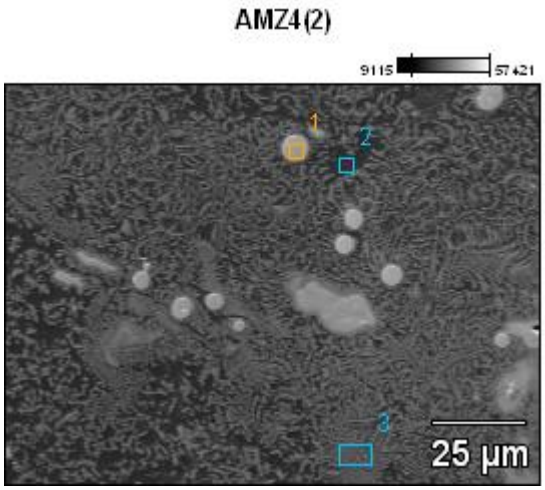

Figure 8. EDX Map area micrograph (AMZ4)

Figure 9 showed the stereo micrograph of sample AMZ 4 alloyed with 50wt%Mo and 50wt% Zr powder. It also indicates the heat affected and the alloyed zones.

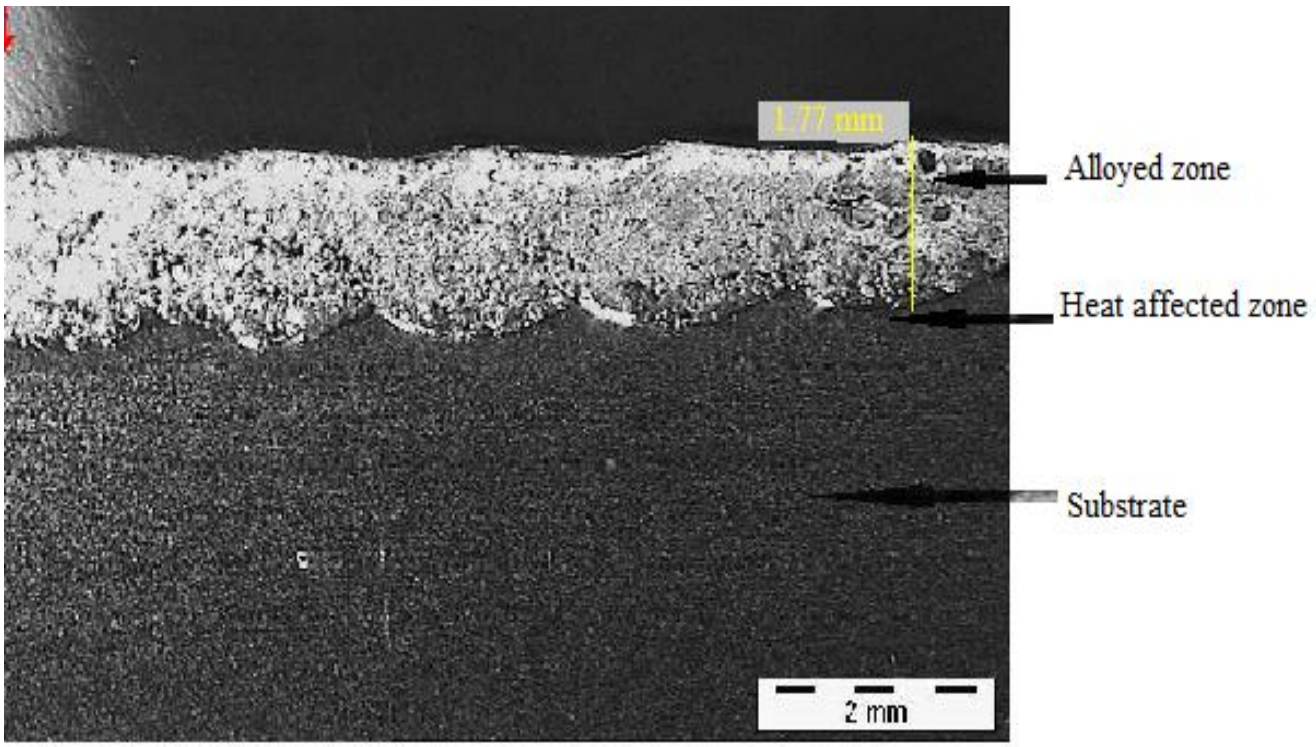

Figure 9. Microstructure of Al alloyed with a mixture of 50wt% Mo and 50wt% Zr powder

The evidence of good metallurgical bond between the substrate and the alloying powders can be seen in figure 9 as a result of homogeneous alloying achieved. Chemical reactions between the substrate and the alloying powder resulted in secondary phases and compound. The maximum depth of the laser alloyed laser was 1.77mm representing 30% of the aluminium substrate thickness.

3.3. Microhardness results

The micro-hardness depth profiles of the three laser alloyed surfaces with 50%Mo and 50% Zr is showed in Figure 10. The hardness values of the samples increase after the laser alloying. This improvement of the hardness values was attributed to the formation of the intermetallic phases after the laser process. From Table 3 and Figure 11 it can be observed that the AMZ 3 exhibited the higher microhardness values. A hardness value of about six times that of the substrate was observed using the combination of Mo and Zr powders. The hardness values obtained depend on the laser parameter used. The optimum conditions were obtained at 50%Mo and 50% Zr, a power of 4 kW and laser scan speed of 1.4 m/min a with a hardness value of 248 HV.

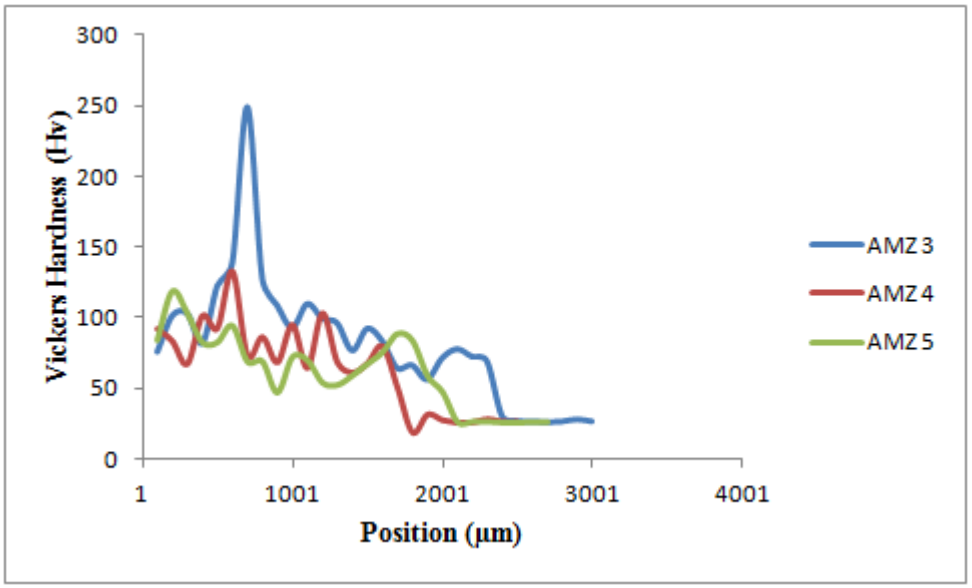

Figure 10. Microhardness depth profile of the alloyed surfaces.

Table 3. Average hardness value of the alloyed surface layers.

Sample name	System composition (Al-Mo-Zr)	Average hardness ($HV_{0.1}$)	Alloyed layer depth (mm)	Laser Scan speed (m/min)
Control	Al	24		
AMZ 3	50% Mo + 50% Zr	148	2.31	1.4
AMZ 4	50% Mo + 50% Zr	103	1.77	1.6
AMZ 5	50% Mo + 50% Zr	75	1.72	1.8

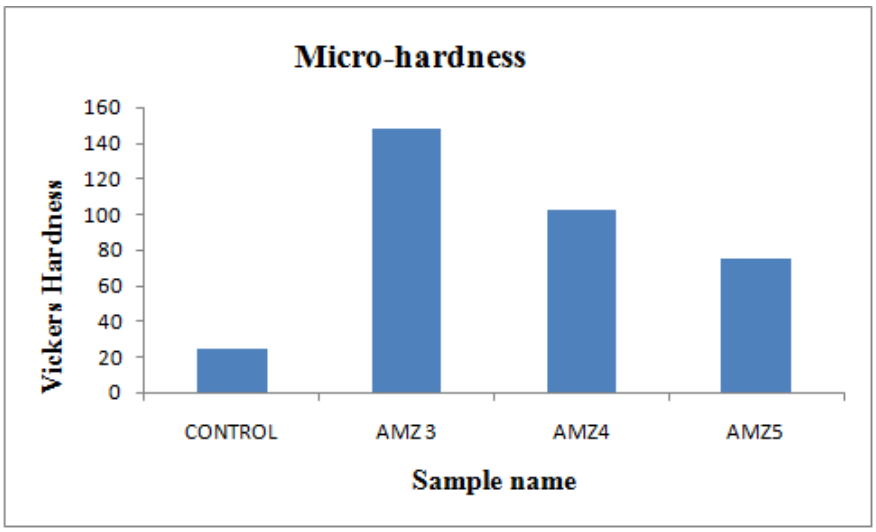

Figure 11. Variation of micro-hardness through thickness

3.4. Wear resistance test result

The results for the mass loss and wear rate for each alloyed sample during the 30 minute wear test duration are shown in Table 4. From Table 4 it may be noted that the wear rate of the samples increased with the decrease in the laser scan speed. From Figure 12, the wear rate of the aluminium substrate is very high compared to the alloyed samples. The alloyed samples contain different secondary phases formed that increase the wear resistance of the coated samples.

Table 4. Wear test results

Sample name	Initial mass (g)	Final mass (g)	Mass loss (g)	Time (min)	Wear rate (g/min)	Scan speed (m/min)
Control	14.27	14.17	0.10	30	$3.33x\ 10^{-3}$	
AMZ 3	11.03	10.95	0.08	30	$2.67x\ 10^{-3}$	1.4
AMZ 4	11.55	11.51	0.04	30	$1.33x10^{-3}$	1.6
AMZ 5	11.16	11.01	0.15	30	$5.00x10^{-4}$	1.8

The wear rates for all the samples after the 30 minute wear test duration are shown in Figure 12 below. The significantly lower wear rate in laser alloyed sample as compared to as-received one is due to an increased hardness of the surface [15]. It was observed that the three samples alloyed with the same metallic powder composition gave different wear resistances. A low wear rate of $5x10^{-4}$ g/min was obtained at a laser scan speed of 1.8 m/min. The poor performance of the coated AMZ 3 sample may be attributed to the Al_3Mo phase present in the coating.

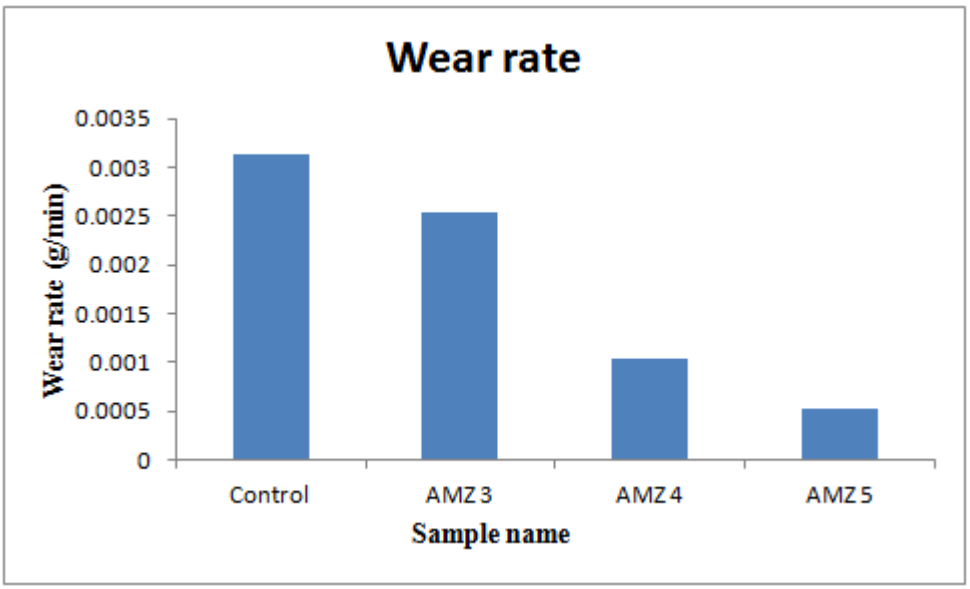

Figure 12. Variation of wear rate with sample name

3.5. Electrochemical test results

Figure 13 and Table 5 summary the results of the corrosion rate for the entire samples.

Table 5. Potentiodynamic polarization data.

Parameter	βa (V/dec)	βc (V/dec)	E_{corr} (V)	I_{corr} (A/cm^2)	R_p (Ω.cm^2)	CR (mm/yr)
Control	0.03	0.98	-1.18	8.29E-04	13.05	9.64
AMZ 3	0.74	1.34	-1.04	1.97E-06	105130	0.02
AMZ 4	0.48	0.47	-1.00	1.54E-05	6813	0.18
AMZ 5	0.07	0.06	-1.07	6.11E-05	233.93	0.71

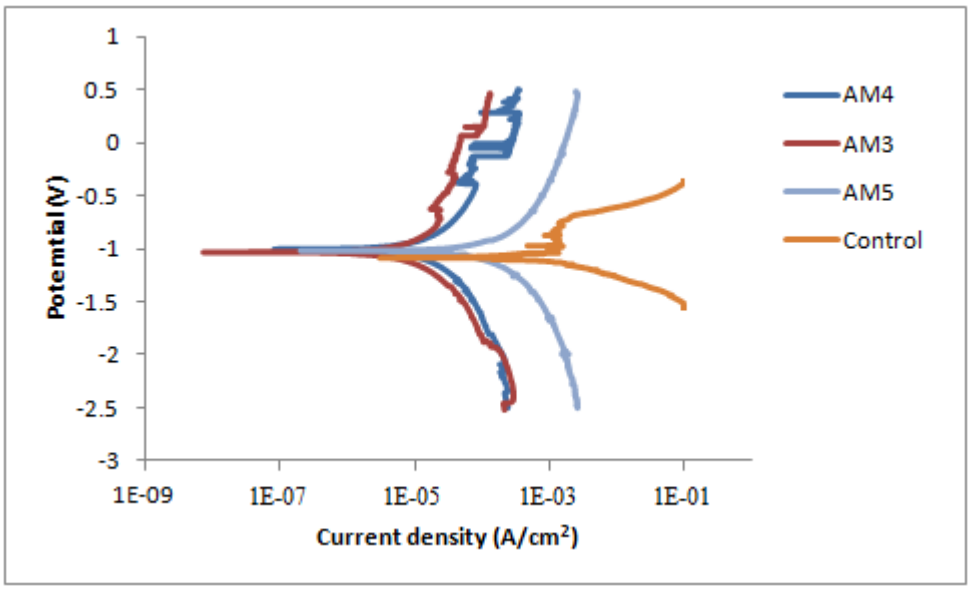

Figure 13. Potentiodynamic curves of Control, AMZ 3, AMZ 4 and AMZ 5 in 3.65 wt.% NaCl.

From Figure 13, it was observed that the AMZ 3 sample exhibited a higher polarization resistance Rp (105130 Ω.cm^2), lowest current density Icorr (1.97x10^{-6} A/cm^2), corrosion potential Ecorr (-1.04 V) and corrosion rate of (0.02 mm/year). The control has the lowest corrosion resistance of all the samples with polarization resistance Rp (13.05 Ω.cm^2), current density Icorr (8.29x10^{-4} A/cm^2), corrosion potential Ecorr (-1.18 V) and corrosion rate of (9.64 mm/year). The AMZ 4 sample exhibited a polarization resistance Rp (6813 Ω.cm^2), current density Icorr (1.54x10^{-5} A/cm^2), corrosion potential Ecorr (-1.00 V) and corrosion rate Cr (0.18 mm/year). Sample AMZ 5 sample exhibited a polarization resistance of Rp (233.93 Ω.cm^2), current density Icorr (6.11x10^{-5} A/cm^2), corrosion potential Ecorr (-1.07 V) and corrosion rate of (0.71 mm/year). The anodic tafel slope βa of the control was the lowest (0.03) followed by AMZ 5 (0.07), AMZ 4 (0.48) and AMZ3 (0.74) respectively. The

cathodic tafel βc of AM5 was the lowest (0.06) followed by AMZ 4 (0.47), control (0.98) and AMZ3 (1.34) respectively. AMZ 3 has the lowest corrosion rate of all the samples.

Lee et al [16] reported Al–Mo as an interesting phase which offers several refractory phases that could be used for strength and stability. The melting point of pure Al is 660 ◦C, while the melting point of pure Mo is 2623 ◦C. Lee et al [16] reported five intermetallic phases of Al-Mo: $Al_{12}Mo$, Al_5Mo, Al_4Mo, Al_8Mo_3, and Al_3Mo. Earlier work had focused on the oxide formation and corrosion properties of Al–Mo synthesized at elevated temperatures (above 700 ◦C), indicating that Al–Mo coatings have far higher corrosion resistance than pure Al [17–22]. From Figure 4, Al_2O_3 corrosion film is chemically inert and its rapid formation of oxide film by a self healing ability leads to a more resistant material in natural environments. Al_2O_3 exhibits excellent corrosion resistance, which decreases the mass loss with increase in their content as reported by Gaitonde et al. [23]. Moreover, the formation of Al_2O_3 oxide layer resists white rust formation. According to Xu et al. [24], the passive layer formed on Inconel 625 is thus believed to mainly consist of Molybdenum oxide. Therefore, the decrease in transpassive potential can be attributed to the effect of MoO_3. The EDS and XRD results from the study also suggested that the improved corrosion resistance of alloys might be due to the formation of MoO_3 and $FeMoO_4$ film on the surface. It can therefore be concluded that an increase in molybdenum content of Cr-Ni-Mo alloys increases the corrosion resistance owing to enhancement of the formation of a molybdenum- enriched passive film [25]. Also, MoO_3 intermetallic is reported to exhibit low friction [26-28].

5. CONCLUSIONS

From the results and discussion above the following conclusions can be deduced:

1. Laser surface alloying with a metallic powder mixture of Mo and Zr resulted in increased hardness and wear resistance.
2. Great improvement in the microhardness of the alloyed surface of 148 $HV_{0.1}$ was achieved in comparison with 24 $HV_{0.1}$ of the substrate hardness.
3. Mo and Zr powder as alloying elements resulted in improved wear resistance by reducing the wear rate to $5.27x10^{-4}$ g/min as compared to $3.13x10^{-3}$ g/ min of the substrate.
4. Mo and Zr powders laser alloyed on AA1200 aluminium substrate showed significant improvement in corrosion resistance compared to ordinary substrate.

ACKNOWLEDGEMENT
This material is based upon work supported financially by the National Research Foundation is based on work supported financially by the (NRF) National Research Foundation. Tshwane University of Technology, Pretoria is appreciated for support which aided the accomplishment of this work.

References

1. R.J. Davis, *ASM int.,* (1999) 10.
2. A. Almeida, M. Anjos, R. Vilar, R. Li and M.G Ferreira, *Surf. Coat. Technol.,* 70 (1995) 221-225.

3. T. G. Rambau, A. P. I. Popoola, C.A. Loto, T. Mathebula and M. Theron*, Int. J. Electrochem. Sci.*, 8 (2013) 5515 - 5528
4. H. S. Campbell, *Copper Development Association Publication*, 80 (1981) 6-22.
5. P.A. Carvalhop, A.M Deus, R. Colac and R. Vilar, *Acta mater.,* 46(5) (1998) 1781-1782.
6. W.J Tomlinson and A.S Bransden, *Wear*, 185 (2013) 59-65
7. A.P.I Popoola, S.L Pityana and O.M Popoola, *Int. J. Electrochem. Sci.*, 6 (2011) 5038-5051.
8. A.P.I Popoola, S.L Pityana, T. Fedotova and O.M Popoola, The *Journal of the South African Institute of Mining and Metallurgy*, 111 (2010) 335-344.
9. L.B.A Mabhali., S.L Pityana and N. Sacks, *Mol. Cryst. Liq. Cryst*., 555 (1) (2012) 138-148.
10. L.B.A Mabhali., S.L Pityana and N. Sacks, *Mater. Manuf. Process*., 25 (2010) 1397-1403.
11. Z. Szklarska-Smialowska, *Corros. Sci*., 33(8) (1992) 1193-1202.
12. M.A McMahon, K.G Watkins, W.M Steen, R. Vilar and M.G.S Ferreira, Surf. Treat. Film Deposition. *NATO ASI Series*, 307 (1996) 337-358.
13. C.W Draper, J.M Poate, *Int. Met. Rev.*, (1995) 1-3.
14. C.W Draper, C.A Ewing, *J. Mater. Sci.*, 19 (1984) 3815.
15. C. Nath, G.C Lim and H.Y Zheng, *Ultrasonics*, 52 (2012) 605-613.
16. Z. Lee, C. Ophus, L.M. Fischer, N. Nelson-Fitzpatrick, K.L. Westra, S. Evoy, V. Radmilovic, U. Dahmen, D. Mitlin, *Nanotechnology*, 17(2006)3063.
17. H. Habazaki, K. Shimizu, P. Skelton, G.E. Thompson, G.C. Wood and X. Zhuo. *Corros. Sci.*, 29(1997)731
18. A.C. Crossland, G.E. Thompson, J. Wan, H. Habazaki, K. Shimizu, P. Skeldon and G.C. Wood. *J. Electrochem.Soc.*, 144(1997) 847
19. M. Janik-Czachor, A. Jaskiewicz, M. Dolata and Z. Werner. *Mater. Chem. Phys.*, 92(2005) 348
20. H. Habazaki, P. Skelton, K. Shimizu, G.E. Thompson and G.C. Wood. *Corros. Sci.*, 37(1995) 1497
21. H. Habazaki, K. Takohiro, S. Yamaguchi, K. Hashimoto, J. Dabek, S. Mrowec and M. Danielewski *Mater. Sci. Eng.* A, 181(1994) 1099
22. W. Wolowik and M. Janik-Czachor. *Mater. Sci. Eng.* A., 267(199) 301
23. V.N. Gaitonde, S.R. Karnik, M.S. Jayaprakash. *J. Miner. Mater. Character. Eng*., 11(2012) 695-703
24. L.Y. Xu, M. Li, H.Y. Jing, Y.D. Han. *Int. J. Electrochem. Sci.*, 8 (2013) 2069-2079.
25. H. Koji, P. Pyeong-Yeol, K. Jin-Han, Y. Hideaki, M. Hiroyuki, A. Eiji, H. Hiroki, K. Asahi, A. Katsuhiko, G. Zbigniew, and M. Stanislaw, *Mater. Sci. Eng.*, 198 (1995) 1.
26. M. Urgen, O.L. Eryilmaz, A.F. Cafir, E.S. Kayali, B. Nilufer, Y. Isik, *Surf. Coat. Technol*., 94–95 (1997) 501.
27. N. Solak, F. Ustel, M. Urgen, S. Aydin, A.F. Cakir, *Surf. Coat. Technol*., 174–175 (2003) 713.
28. T. Suszko, W. Gulbinki, J. Jagielski, *Surf. Coat. Technol*., 194 (2005) 319.